Choupani Chaydarreh *et al.*
Journal of Wood Science (2024) 70:32
https://doi.org/10.1186/s10086-024-02144-2

Journal of Wood Science

ORIGINAL ARTICLE

Open Access

Developing a lightweight corrugated sandwich panel based on tea oil camellia shell: correlation of experimental and numerical performance

Kamran Choupani Chaydarreh[1,2], Jingyi Tan[1], Yonghui Zhou[1*], Yongtao Li[2] and Chuanshuang Hu[1*]

Abstract

This study presents an experimental and numerical comparison between the mechanical performance of a lightweight corrugated sandwich panel based on the tea oil camellia shell (TOCS). Hence, TOCS was mixed in two groups with Poplar particles and fibers. After that, in the experimental part, the conventional mechanical tests, including the 3-point bending test, flatwise compression, dowel bearing, and screw resistance, and in the numerical part, finite element analysis (FEA), including the normal, maximum principal, and equivalent (von Mises) stress by Ansys Mechanical software carried out. The specimens for experimental and numerical tests were prepared in transverse and longitudinal directions. Before that, the engineering data (shear modulus, Young's modulus, and Poisson's ratio) for improving the FEA simulation were obtained from TOCS-based flat panels fabricated with a mixture of Poplar particles and fibers. The results of FEA are used to compare the mechanical behavior and failure mechanism with the results of experimental tests. According to the mean values of bending stiffness and maximum bending moment, sandwich panels made with 100% particles demonstrated an advantage in both directions. Nevertheless, the compression strength and screw resistance showed the same trend, but the dowel bearing showed higher values for panels made with fibers. The observed results of equivalent (von Mises) stress indicated a coloration with the results of failure mechanisms.

Keywords Sandwich panels, Tea oil camellia shell, Corrugated structure, Particleboard, Fiberboard

Introduction

Sandwich panels provide excellent mechanical properties compared with their lightweight and require low maintenance costs, while can be utilized in a variety of complex projects. Concerning the mentioned advantages, the usage of these engineering products has grown steadily in the construction, transportation, aerospace, automotive, and marine industries [1, 2]. In the last decades, wood has played a vital role in the development of new sandwich panels [3]. Therefore, different types of raw wood or wood composites in a variety of geometries have been investigated by numerous studies. These structures mainly were distinguished by foam core particleboard [4], honeycomb core [5], low-density wood species [6], interlocking lattice core [7], modified wool-polypropylene [8], cork agglomerate [9], and so on. In addition to the aforementioned structures, corrugated core layer with a lightweight structure, excellent strength, high stiffness, and shock resistance properties showed relative

*Correspondence:
Yonghui Zhou
y.zhou@scau.edu.cn
Chuanshuang Hu
cshu@scau.edu.cn
[1] College of Materials and Energy, South China Agricultural University, Guangzhou 510642, China
[2] College of Natural Resources and Environment, South China Agricultural University, Guangzhou 510642, China

superiority compared to other sandwich structures [10]. In this context, various approaches have demonstrated functional results, including corrugated structure with wood veneer [11], biaxial corrugated core based on low-quality spruce-pine-fir strands [12], sinusoidal corrugated concept for the core layer of plywood sandwich panels [13], forming the Black cherry (*Prunus serotina*) veneer into corrugated structure [14], and corrugated sandwich panel based on balsa wood stands [15].

According to the FAO report, from 2018 to 2022, China produced 30 million cubic meters of particleboard each year, and a recent study has reported that the production of one cubic meter of particleboard required about 1216 kg of wooden raw materials [16]. Therefore, the circular economy (CE) concept has led academia and industry to develop the construction materials based on using sustainable or unused agricultural wastes. A considerable amount of information is available regarding the fabrication of conventional flat wood-based panels using agricultural wastes [17]. However, severely limited literature exists regarding to corrugated panels based on agricultural wastes. In this direction, tea oil camellia shell (TOCS) as a by-product of oil extraction has the potential to provide approximately 4 million tons of raw materials every year in the southern province of China and it is undergoing continuous expansion [18]. These abandoned raw materials were introduced as a viable alternative resource for manufacturing wood-based panels, particularly particleboards [19, 20], which are traditionally produced in a flat shape with a variety of thicknesses. Concerning that fact, utilization of TOCS for a new shape configuration of sandwich panels can be a beneficial way regarding to high strength and stiffness of sandwich structure [21]. The geometry configuration of the corrugated core has a significant impact on the ultimate strength, failure mode, and impact-absorbing capabilities of sandwich panels [22, 23]. The corrugated cores have few prevalent geometries, including the arc-shaped core, sinusoidal core, rectangular core, trapezoidal core, and triangular shape [24].

This study aims to provide an eco-friendly sandwich panel with a lower density than conventional wood-based panels but with higher mechanical properties for structural application. Specifically, aligning with the CE concept, trapezoidal corrugated sandwich panels were developed based on TOCS particles in combination with Poplar (*Populus*) particles or fibers. The work has been focused on achieving a complete understanding of the mechanical behavior and failure mechanism of the newly developed corrugated lightweight sandwich panels by conducting comprehensive experimental and numerical analyses. In the experimental part, mechanical properties including the quasi-static bending strength, flatwise compression, dowel bearings, and screw resistance were tested on samples prepared in transverse and longitudinal directions by following ASTM criteria. The numerical part was carried out with the help of finite element analysis (FEA), which is a computerized method for predicting how a material reacts to real forces. To improve the accuracy of numerical modeling, engineering data (shear modulus, Young's modulus, and Poisson's ratio) were measured for each panel type in this study. SolidWorks software was used to develop the 3D geometries of trapezoidal corrugated panels, and Ansys Mechanical software was used for performing the FEA in terms of the normal stress, maximum principal stress, and equivalent (von Mises) stress.

Materials and methods

Raw materials and preparation

The TOCS was sourced from a camellia oil factory and the Poplar (*Populus*) fibers and particles were sourced from a local factory in Guangdong province, China. Polymeric methylene diisocyanate (pMDI) of Wanhua Chemical Group, Yantai, China with a solid content of 99.2%, a viscosity of 150–250 mPa s, and a density of 1.22–1.25 g/cm^3 at 25 °C was used as a resin for fabricating the flat and corrugated panels. To assemble the sandwich structure, conventional polyvinyl acetate (PVA) was used. TOCS were chipped using a grinder (Grinder CM200, Beijing Grinder Instrument Co., Ltd., Beijing, China), and the particles were then screened according to ASTM standards with a mesh size of + 3 to − 30. For achieving an approximate moisture content of 3%, all raw materials were oven dried for 24 h at 65 °C. Figure 1 shows the raw materials used in this research.

Fabrication of flat and corrugated panels

Flat panels

In this study, all panels (flat and corrugated) were manufactured by a computer-controlled laboratory hot press (XINXIELI Enterprise Development Co., Ltd., Suzhou, China), with a density of 580 kg/m^3 (lightweight panels based on ASTM D1554 [25]) and a nominal thickness of 10 mm. Using a ratio of 50% TOCS particles to 50% Poplar particles or fibers, two concepts of panels (particle based (PBP) and fiber based (FBP)) were fabricated. The particles and fibers were resonant with 6% pMDI in a rotary lab blender, while their moisture was adjusted to 10% by spraying water. Following that, the materials were formed into a square box measuring 480 × 480 mm^2. A manual pre-pressing was performed and hot-pressing was adjusted to be 200 s with a picking pressure of 3.5 MPa and a temperature of 180 °C.

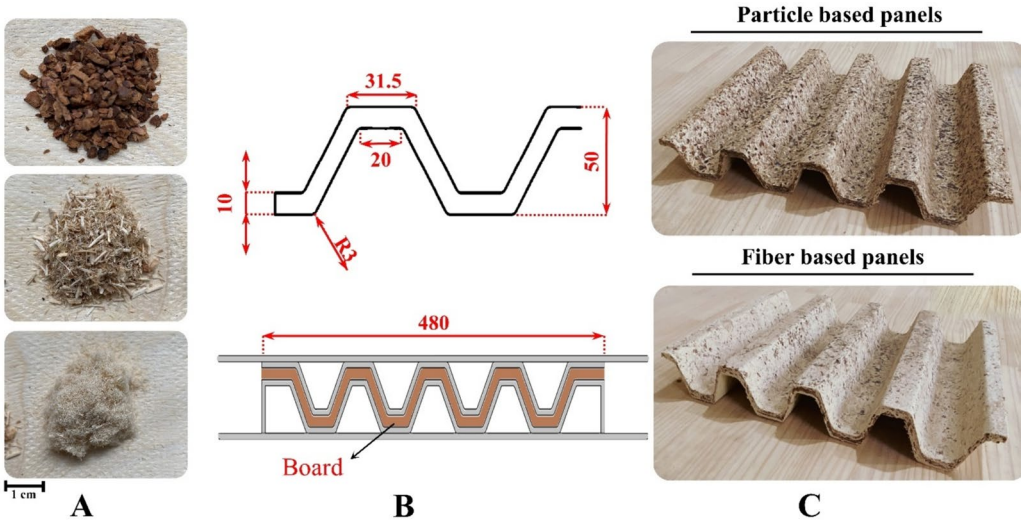

Fig. 1 **A** Raw materials used in this study, **B** Details of trapezoidal corrugated mold, **C** Fabricated panels (unit: mm)

Corrugated panels

For the fabrication of corrugated panels, the hot-pressing variables, mixing ratio, and resin content were similar to those for flat panels. The materials mixture was formed into a box and then transferred via aluminum foil into a trapezoidal corrugated mold that was already connected to the hot-press machine. A detailed description of the corrugated mold and the produced corrugated panels is shown in Fig. 1.

Assembly of corrugated sandwich panels

In the following steps, the corrugated core was attached to flat panels with a thin layer of PVA glue (400 g/m^3) which is a conventional type of adhesive for furniture manufacture and joinery, and assembled sandwich panels were placed into a cold press which adjusted with a 7 cm distance between plates until glue curing (2 h) completed. Later, the sandwich panels were cut into specimens for mechanical test and conditioned for seven days in a climatic chamber at 20 °C and 65% relative humidity.

Characterization of flat and corrugated panels

ASTM standards were used to characterize several necessary mechanical properties of flat and corrugated sandwich panels, six specimens were considered for each test. The mechanical properties were measured using a universal testing machine (CMT5504, Shenzhen Rethink Cooperation, Shenzhen, China).

Flat panels

Bending strength (modulus of rupture (MOR) and modulus of elasticity (MOE)), internal bonding (IB), and face screw withdrawal resistance (FSW) were measured according to ASTM D1037 [26]. As required by the testing protocol, specimens for bending strength were prepared in the dimension of 290×76×10 mm^3; while for the other tests, square specimens were prepared in the dimension of 50×50×10 mm^3. Moreover, the shear modulus (G) and Young's modulus (E) plus Poison's ratio (υ) of flat panels were obtained using ASTM D3044 [27] and ASTM D1037 [26], respectively, as a requirement for FEA. Figure 2 shows the test setup for measuring these parameters. The tests were conducted following the XYZ axes of flat panels and six specimens were considered for each test. To determine the shear modulus the Eq. (1) and Young's modulus the Eq. (2) were used.

$$G = \frac{3u^2P}{2h^3\Delta}, \tag{1}$$

where G is the shearing modulus (MPa), u is distance from the center of the panel to the point where the deflections are measured (mm), P is load applied to each corner (N), h is thickness of the panel (mm), and Δ is deflection relative to the center (mm).

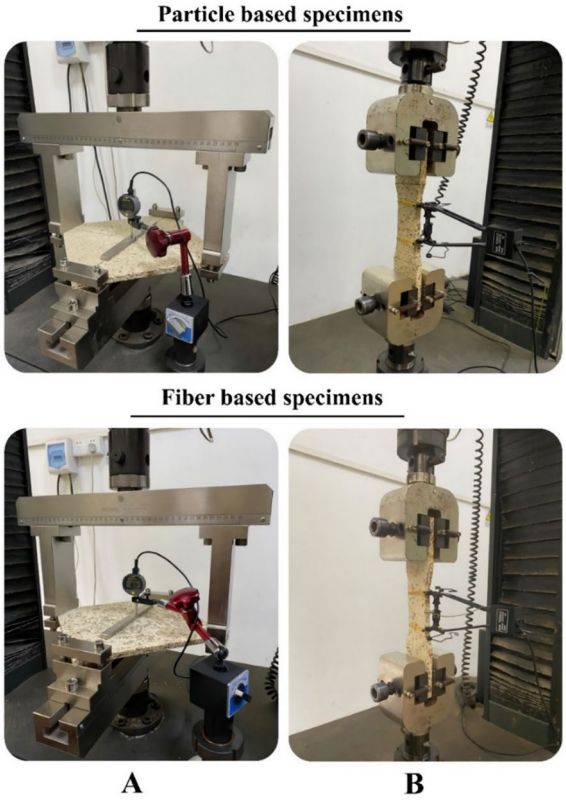

Fig. 2 Test setup for FEA requirements, **A** Shear modulus test; **B** Tension parallel to surface test to obtain Young's modulus and Poisson's ratio

$$E = \frac{lg}{bd} \times \frac{\Delta p}{\Delta y}, \tag{2}$$

where lg is gage length or distance between the gage points of extensometer (mm), b is width of the reduced cross section of the specimen measured in dry condition (mm), d is thickness of specimen measured in dry condition (mm), and $\frac{\Delta p}{\Delta y}$ is slope of the straight-line portion of the load–deformation curve (N/mm).

Corrugated sandwich panels

Before assembling the sandwich panels, tensile test was conducted on the corrugated panels by ASTM D1037 [26]. To study the tensile strength of the core layer, samples with dimensions of 254×51×10 mm^3 were prepared according to standard procedures and this property was calculated according to Eq. (3).

$$R = \frac{P_{\max}}{bd}, \tag{3}$$

where R is maximum tensile stress (MPa), $P_{\max}$ is maximum load (N), b is width of the reduced cross section of specimen (mm), and d is the thickness of specimen (mm).

Later on, according to ASTM D3043 [28], quasi-static three-point bending test was conducted on samples which prepared in transverse and longitudinal directions (Fig. 3). The sample size for bending test 330×110×70 mm^3 and using Eqs. (4) and (5), the bending stiffness (EI) and maximum bending moments (FbS) were calculated, respectively. It must be noted that some adaptations are considered due to the particular shape of the corrugated panels.

$$\mathrm{EI} = \frac{P \times L_s^3}{\Delta \times 48 \times b}, \tag{4}$$

$$\mathrm{FbS} = \frac{P \times L_s^3}{4 \times b}, \tag{5}$$

where EI is bending stiffness (N-mm^2 / mm), P is the load applied (N), L_s is the span length, Δ is the deflection (mm), b is specimen width (mm), and FbS is maximum bending moment (N-mm / mm).

The core shear ultimate strength of sandwich panels was calculated in accordance with ASTM C393 [29] using Eq. (6).

$$F_s^{\mathrm{ult}} = \frac{F_{\max}}{(d+c)b}, \tag{6}$$

where F_s^{ult} is core shear ultimate strength (MPa), d is sandwich panel thickness (mm), c is core layer thickness (mm), and b is sandwich panel width (mm).

Additionally, flatwise compression was conducted based on ASTM D143 [30]. The sample size of 110×110×70 mm^3 was considered for sandwich panels and 110×110×50 mm^3 for the corrugated panels. The test setup is shown in Fig. 3. Using the load and crosshead deflection data, compressive stress was calculated according to Eq. (7).

$$\sigma = \frac{P_{2.5}}{\mathrm{A}}, \tag{7}$$

where σ is compressive stress, $P_{2.5}$ is load (N) at 2.5 mm of compressive displacement, and A is total area of the facing (mm^2).

To assess the performance of fasteners, a sample size of 110×110×70 mm^3 was prepared for each test. Initially, ASTM D5764 [31] was used to assess the dowel-bearing properties of sandwich panels in two directions of vertical and horizontal to corrugated geometry. This was accomplished using a dowel with a diameter of 10 mm. Additionally, the FSW resistance was determined according to ASTM D1761 [32] standard.

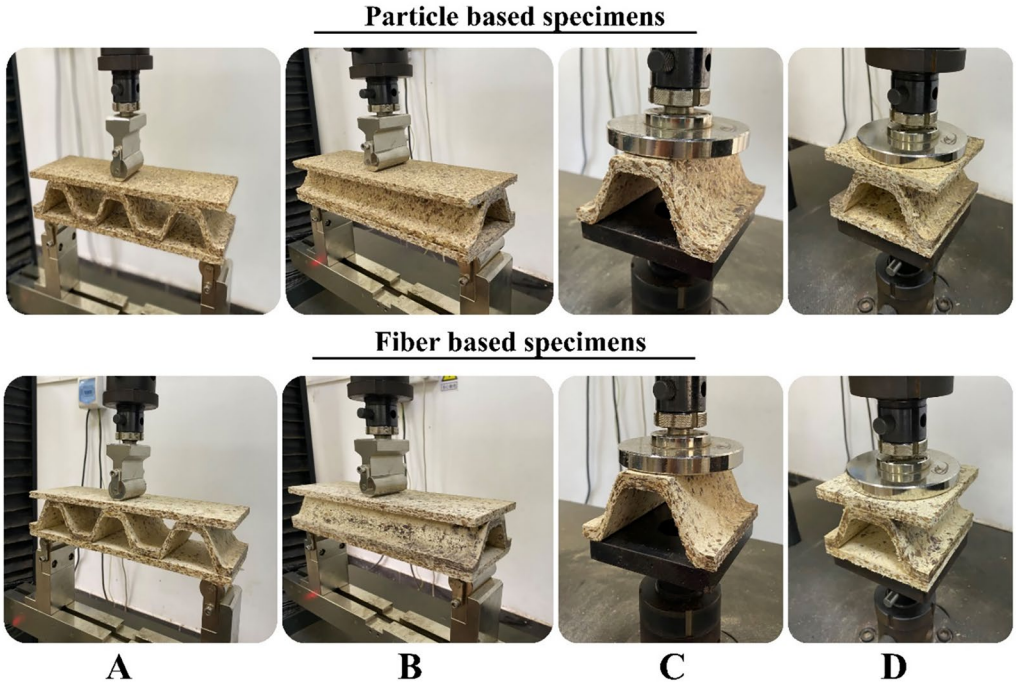

Fig. 3 Test setup for quasi-static bending (**A** Transverse and **B** Longitudinal direction) and flatwise compression (**C** Corrugated panels and **D** Sandwich panels)

Finite elements analysis

The most commonly used simulation method in science and engineering research is FEA, which can predict the mechanical performance of a material through computer modeling, and it is an effective tool for optimizing parameters during the design process. Thus, by adopting Ansys Mechanical software, the normal stress, maximum principal stress, and equivalent (von Mises) stress are simulated for both panel types. The purpose of these simulations was to compare panel types in terms of bending performance and achieve a better understanding of the mechanical behavior and failure mechanisms. The samples were designed for FEM simulation in 2 directions (transverse and longitudinal) with a 280 mm distance between the center of spans. The load was applied in the center of upper surface with a half-cylinder which had 70 mm length and 28 mm diameter. To perform the FEA simulations, segmented 3D models with complex microstructural arrangements need to be discretized into geometry-based tetrahedral mesh structures. For discretizing each sample, the three-dimensional SOLID185 elements were used with eight nodes and three degrees of freedom per node

Table 1 Deflection to each mesh applied to check the computational modeling convergence

Mesh size (mm)	PBP				FBP			
	Transverse direction		Longitudinal direction		Transverse direction		Longitudinal direction	
	Elements number	Def. (mm)	Elements number	Def. (mm)	Elements number	Def. (mm)	Elements number	Def. (mm)
20	1254	7.15	1246	2.23	1254	4.99	1246	1.68
15	1526	7.24	1502	2.42	1526	5.09	1502	1.83
10	2976	7.26	2238	2.78	2976	5.19	2238	2.09
5	13,316	7.42	10,910	3.31	13,316	5.26	10,910	2.50
3.3	49,350	7.74	46,194	3.68	49,350	5.45	46,194	2.89
2.5	90,778	7.81	80,158	3.75	90,778	5.53	80,158	2.94

Def. is deflection

(translation according to *X*, *Y*, and *Z* axes), and stiff adhesion was considered between corrugated core and flat surfaces (without slippage). Different variations of mesh sizes (20, 15, 10, 5, 3.3, and 2.5 mm) were applied to understand the effect of mesh size on element numbers and deflection (Table 1). By decreasing the mesh size, more accurate results could be obtained; however, it may increase the computational analysis duration [33]. After applying each mesh size, the specimen deflection was measured using a bending test. This step was intended to ensure mesh size does not significantly affect specimen properties. According to the observed results, mesh 3.3 and 2.5 mm showed a similar deflection regardless of specimen direction or raw material type. As a result, the mesh size for the geometry structure (trapezoidal) in this study was 3.3 mm. By selecting this mesh size, it is possible to optimize processing time and obtain accurate output. In addition, the simulation was solved using a number of 10 load steps with an end time of 1 s in to match the quasi-static loading condition. The engineering data for simulating PBP and FBP were taken from Table 2. For the load cell and spans, due to their materials, structural steel (Density: 7850 kg/m^3, Poisson's ratio: 0.3, shear modulus: 76,923 MPa, and Young's modulus: 200,000 MPa), which is the default material of Ansys Mechanical software was adjusted.

Specific energy absorption

The specific energy absorption (SEA) is the energy absorption ratio to the sandwich specimen's mass [34] and commonly used to characterize the bending and compression worthiness of a structure with the help of Eqs. 8 and 9.

$$\mathrm{SEA} = \frac{E}{\mathrm{m}}, \tag{8}$$

$$E = \int_0^{\mathrm{def}} F(x)dx, \tag{9}$$

where E is the energy absorbed by specimen (J), m is the mass of specimen (g), def is the specimen deflection (mm), and $F(x)$ is the maximum load (N).

Statistical analysis

Two-sample *t*-tests were performed to investigate differences between variables at the 5% significance level. All analyses were performed using SPSS (Statistical Package for the Social Sciences) software.

Results and discussion

Engineering data of flat panels for FEA

The results of engineering data measured of flat panels are demonstrated in Table 2. To simplify the analysis for the orthotropic model, the properties for thickness direction (*Z*-axis) are considered to be 10 times smaller than those experimentally obtained in the *X*-axis [35]. It was observed that FBP had a higher Young's modulus than PBP along all axes. In general, fibers may provide better mechanical properties in terms of elasticity as a result of their morphology, which is primarily determined by their aspect ratio and their content of cellulose [36]. A higher Young's modulus induced higher strain, which resulted in a higher Poisson's ratio (the ratio between transverse and axial strains); hence, this phenomenon can be described by a higher aspect ratio and likely lower lignin content of fibers. A similar trend was observed in the results of the shear modulus, the PBP indicated a value of 311 N/mm^2; whereas, the FBP indicated a value of 351 N/mm^2. Alternatively, FBP's higher values in observed data could be also explained by the density of the panels. Whereas, the mean value for PBP's appearance density was 563 kg/m^3 and the average density for FBP was 588 kg/m^3.

Table 2 Engineering parameters of TOCS-based flat panels

Panel type	Density (kg/m^3)	Test direction	Young modulus *E* (N/mm^2)	Poisson's ratio (*υ*)	Shear modulus *G* (N/mm^2)
PBP	563	*X*-axis	930 (7.6)	0.12 (2.1)	311 (9.3)
		Y-axis	578 (8.4)	0.15 (2.4)	
		Z-axis	93 (7.3)	0.15 (2.4)	
FBP	588	*X*-axis	1363 (15.4)	0.18 (1.9)	351 (4.1)
		Y-axis	759 (16.3)	0.21 (2.7)	
		Z-axis	136 (14.8)	0.21 (2.7)	
Sample size (mm^3)			254 × 51 × 10	254 × 51 × 10	260 × 260 × 10

The values in parenthesis are COV%

Table 3 Mechanical characterization of flat panels

Test type	MOE (N/mm^2)	MOR (N/mm^2)	IB (N/mm^2)	FSW (N)
PBP	825 (17.9)	4.98 (3.9)	0.77 (6.6)	499 (14.2)
FBP	870 (11.7)	3.95 (3.6)	0.72 (7.1)	545 (12.7)
LD-1* (ANSI A208)	500	2.8	0.10	360

The values in parenthesis are COV%

* LD-1 stands for low-density panels (generally less than 640 kg/m^3)

Mechanical properties of flat panels

Table 3 presents the mean values for the common mechanical properties of flat panels. Understanding the mechanical properties of flat panels as a part of sandwich structure may provide useful information for further discussion. The results of bending strength test indicated that PBP could have better properties in MOR, while FBP demonstrated a higher elastic response, resulted in slightly higher MOE. It should be noted that both panel types demonstrated similar IB strength; however, results of Korai et al. indicated slightly higher IB in fiberboard [37]. It was found that fibers due to higher aspect ratio than particles could provide a higher mean value when it came to screw holding [38]. In summary, all properties of PBP and FBP met the minimum requirement for a lightweight panel according to ANSI A208 [39] (Table 3).

Tensile and ultimate strength of corrugated geometry

According to mean values of maximum tensile stress (Table 4), PBP samples indicated a tensile stress of 0.46 MPa with a COV of 7.3%, and this value for FBP samples was 0.35 MPa with a COV of 6.8%. All samples exhibited a failure behavior upon tension, where specimens flattened toward the loading handles, and then collapsed completely until failure occurred in the reduced section. It should be noted that the slope area of corrugated in FBP samples had lower strength, consequently, failure occurred with a lower tensile load. The reason behind this phenomenon could be due to an inappropriate mixture of fibers with TOCS particles, which probably caused some of the raw materials to lose access to contact with the adhesive. The FEA results for the tensile simulation of corrugated panels are indicated in Fig. 4. The equivalent (von Mises) stress for PBP and FBP revealed a coloration between numerical and mechanical tests. There is a maximum tension in the reduced section of specimens that failure occurred in that region. In alignment with that, the higher tension (yellow color) is more dominant for FBP. However, using fibers for flat panels indicated higher tensile properties than those fabricated

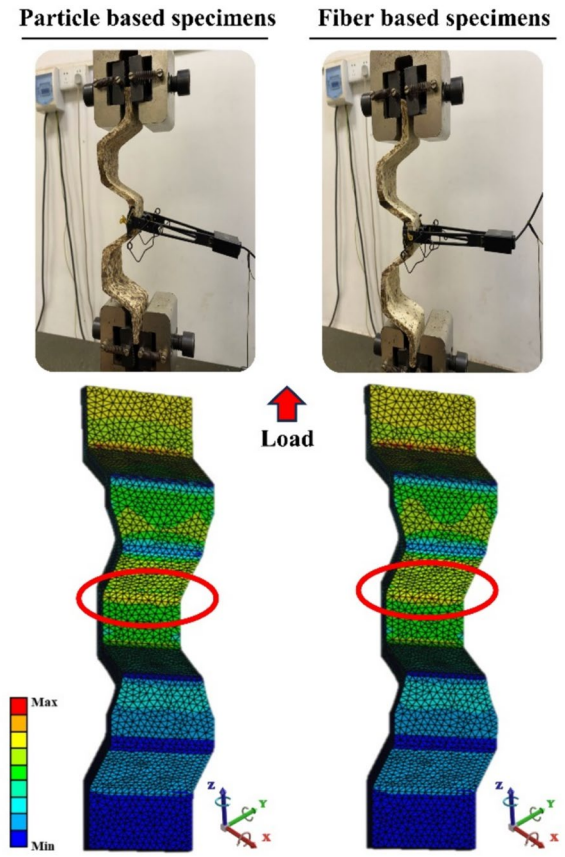

Fig. 4 Test setup and FEA simulation of tensile properties for corrugated panels

Table 4 The quasi-static 3-point bending tests

Treatment	Direction	F_{max} (N)	EI (N-mm^2/mm) (×10^6)	FbS (N-mm/mm)	Deflection (mm)	Tensile stress* (MPa)
PBP	Transverse	1596 (4.6)	2.27 (3.5)	1015 (4.5)	2.92 (5.9)	0.46 (7.3)
	Longitudinal	1664 (7.5)	2.01 (4.9)	1059 (7.4)	3.45 (3.6)	
FBP	Transverse	1430 (9.9)	2.21 (7.4)	893 (8.8)	2.63 (3.3)	0.35 (6.8)
	Longitudinal	1566 (6.2)	1.78 (6.4)	996 (6.2)	3.66 (5.7)	

The values in parenthesis are COV%

* The results of tensile stress were considered just for corrugated panels

by particles. The tensile results of a corrugated structure suggested that a mixture of TOCS particles with Poplar particles would provide stronger slopes in this structure. In addition, results of core shear ultimate strength indicated a value of 0.127 and 0.121 MPa for transverse and longitudinal PBP samples and 0.119 and 0.108 MPa for FBP specimens. These results also may be related to the geometry of raw materials. The weaker slope strength in corrugated panels made with fibers is caused by a lower ultimate strength.

Mechanical properties of corrugated sandwich panels

Quasi-static bending properties

The mean value of the bending stiffness and maximum bending moment are presented in Table 4. After comparing the results, it was found that F_{max} either for PBP (1664 N) or FBP (1566 N) had higher values for samples prepared in longitudinal direction. Regarding linear relations between load and deflection, the samples subjected to bending force exhibited changes in Z axial direction until failure [40]; hence, higher F_{max} for samples prepared in longitudinal direction resulted in slightly higher deflection compared with transverse direction Fig. 5A. In general, deflection is linearly proportional to the applied load, meaning that higher loads lead to greater deflection [40] and consequently as deflection is an influential variable (Eq. 4), higher deflection could result in lower bending stiffness of a sandwich panel. The mean values of bending stiffness for PBP were 2.01×10^6 N-mm^2/mm for longitudinal samples and 2.27×10^6 N-mm^2/mm for transverse samples, while these values for FBP were 1.78×10^6 and 2.21×10^6 N-mm^2/mm, respectively. In the elastic range, the total deflection of a sandwich panel can indicate its stiffness. Regarding maximum bending moment, PBP demonstrated superior values compared with FBP. The mean value of FbS for PBP indicated 1059 N-mm/mm in longitudinal and 1015 N-mm/mm in transverse samples. These values for FBP showed about 10% lower. Higher FbS value for longitudinal samples of trapezoidal corrugated sandwich panels was also reported by other studies focused on trapezoidal corrugated structure [15, 41]. It is worth to mention that the sandwich panels in this study are mechanically (bending stiffness and maximum moments) suitable for use as structural material based on the criteria classified in APA PS 2–10. In this class, bending stiffness was determined

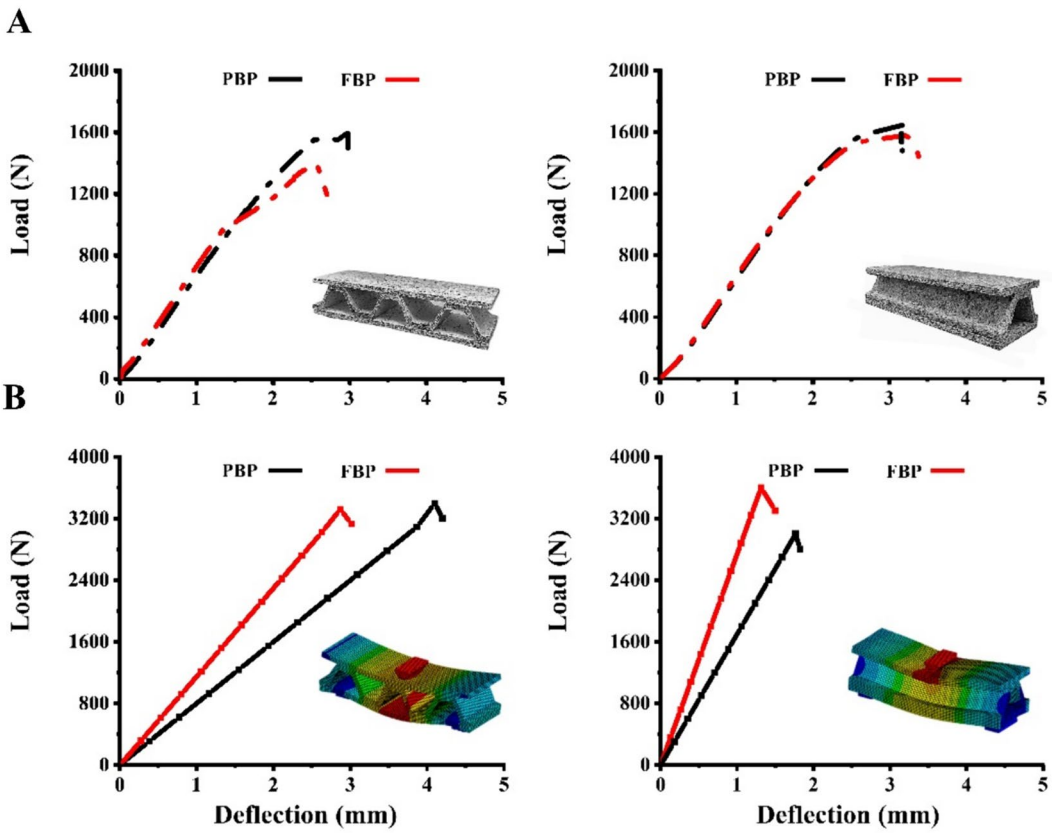

Fig. 5 Load–deflection graphs, **A** Bending test and **B** FEA simulation

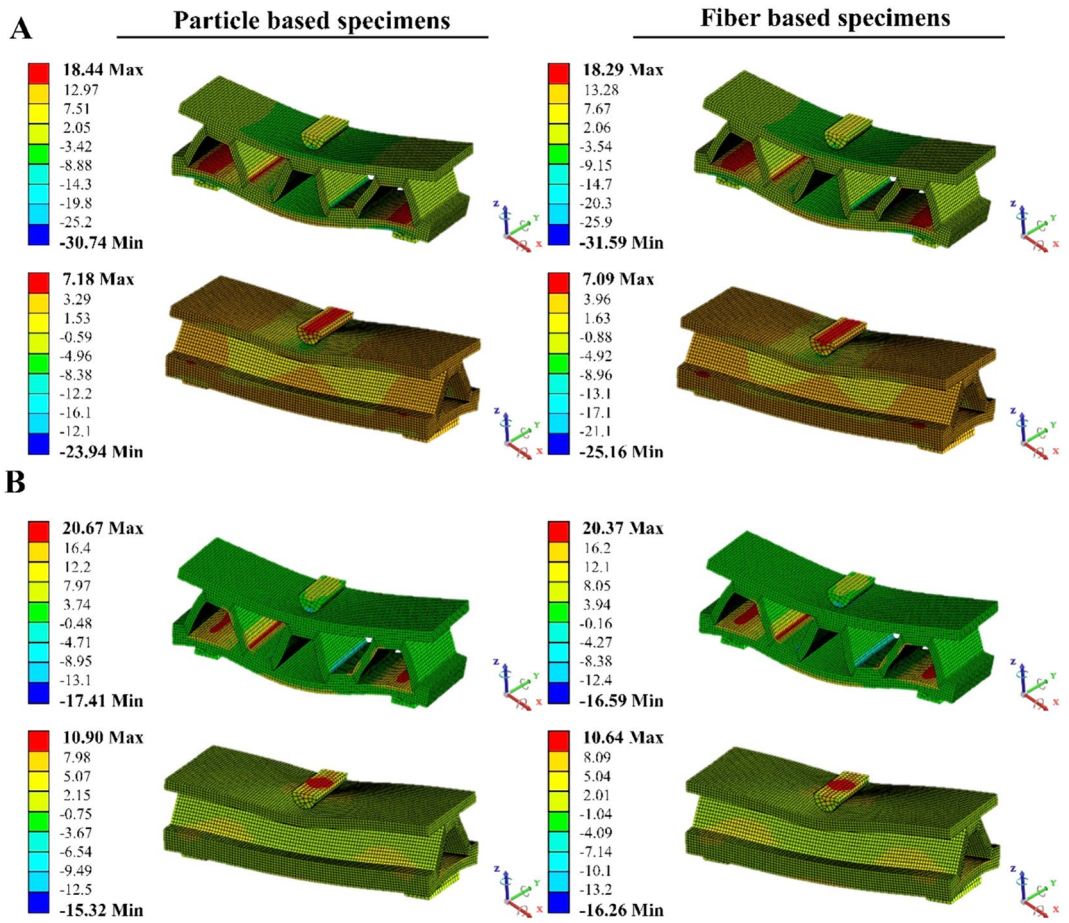

Fig. 6 Bending properties simulation by FEA, **A** Normal stress and **B** Maximum principal stress

to be 0.7 and 1.8 (N-mm^2/mm) for TD and LD, respectively. In addition, the FbS was determined to be 650 and 920 (N-mm/mm) for TD and LD, respectively.

To simulate the bending performance of corrugated sandwich panels, normal stress, and maximum principal stress (Fig. 6) were run on 3D specimens in both transverse and longitudinal directions. The FEA method was carried out to achieve a better understanding of different raw material behavior and comparison with actual mechanical tests. The maximum tension stress is shown in red. According to the obtained results of normal stress, the concept of a corrugated sandwich panel based on TOCS mixed with poplar particles indicated slightly better performance than those with fibers. The structure of transverse samples appeared to have a higher number of maximum tension regions with failure potential. The same trend was observed in terms of maximum principal stress. PBP was capable of bearing more tension in both directions. It is noteworthy that maximum tension stress for transverse samples occurred primarily in the bottom region around the support area as well as at the corner region of the trapezoidal core slope area of corrugated that bonded to the bottom flat panel. Additionally, when it comes to longitudinal samples, maximum tension stress occurred primarily at the support area and center of the panels in the bottom flat panel. Moreover, the results of the bending stiffness and maximum moment agree with the results of the normal stress and maximum principal stress.

In a sandwich panel, the total deflection is made up of bending components (surface layers) and shear components (core layers). As shown in Fig. 5B, the maximum deformation (numerically) for PBP and FBP was higher for samples prepared in transverse direction. These results were opposite to obtained deflection of bending test (Table 4). A reason for this phenomenon could be related to density distribution, in laboratory scale is hard to control density distribution of panels and it may affect the mechanical properties of sandwich panels. In the study about OSB sandwich panels manufactured with trapezoidal core, the same phenomenon was reported [15].

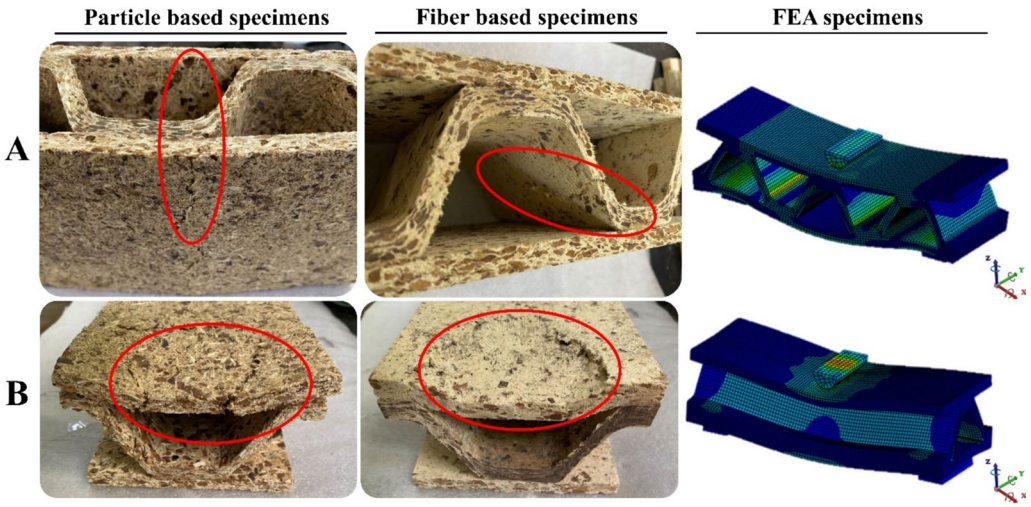

Fig. 7 Failure map of bending test, **A** Transverse direction and **B** Longitudinal direction

The failure map for the bending test is shown in Fig. 7. As can be seen, the different failure mechanisms were observed for transverse samples. The failure in PBP samples was due to a rip across the bottom layer. This type of failure is classified as type (C) according to ASTM C 393 [29]. The undamaged corrugated core indicated the excellent bending properties of this structure with poplar particles. It is interesting to mention that in the concept of a sandwich, generally, surface layers have a higher density than core layers [42]. While in this study, the core and surface layers were fabricated in even density. Hence, increasing the density of flat panels can significantly improve the bending properties of corrugated particleboards. On the other hand, the failure in FBP samples occurred at the slope area of corrugated, which is classified as a type (F) failure. Most likely mixing Poplar fibers with TOCS particle resulted in weak slope for the corrugated core due to different geometry and aspect ratio [43]. In samples prepared in longitudinal (Fig. 7B), the failure mechanisms indicated similar mode for the PBP and FBP. The failures occurred at the region where samples were placed on the span supports (bottom layer). An explanation for this type of failure could be related to the smaller size of spans than the sample width. Interestingly, the failure mechanism was correlated with the maximum tension stress observed in FEA calculations. The failure maps of samples prepared in transvers direction was similar to region with maximum tension based on equivalent (von Mises) stress (Fig. 7C). The FEA method is useful for the analysis of the failure mechanism in complex structures such as a corrugated sandwich panel [44].

Flatwise compression properties

The results of the flatwise compression test for corrugated and sandwich panels are presented in Table 5. Considering the corrugated panels used as the core, after the force reached the maximum moment, the specimens gradually collapsed at slope area of corrugated (for both panel types). The mean values indicated 0.39 MPa with a COV of 9.1% for PBP and 0.25 MPa with a COV of 8.6% for FBP. The difference may be attributed to the fact that particles are able to provide a stronger slope in the trapezoidal corrugated structure than fibers, and thus, PBP could provide a better flatwise compression. Regarding the results of corrugated sandwich panels, the mean values indicated the same trend as mentioned above. The compression strength for PBP was 0.63 (8.9%), and for FBP was 0.45 (8.4%). Burrito et al. reported a compression strength of 0.77 MPa for corrugated sandwich panels fabricated with

Table 5 The mean value of mechanical tests for TOCS-based sandwich panels

Panel type	Compression strength (MPa)		FSW resistance (N)	Dowel bearing (N)	
	Corrugated panel	Sandwich panel		Vertical	Horizontal
PBP	0.39 (9.1)	0.63 (8.9)	2249 (7.8)	6853 (9.3)	2826 (12.2)
FPB	0.25 (8.6)	0.45 (7.4)	2204 (9.5)	8076 (11.4)	3271 (8.6)

The values in parenthesis are COV%

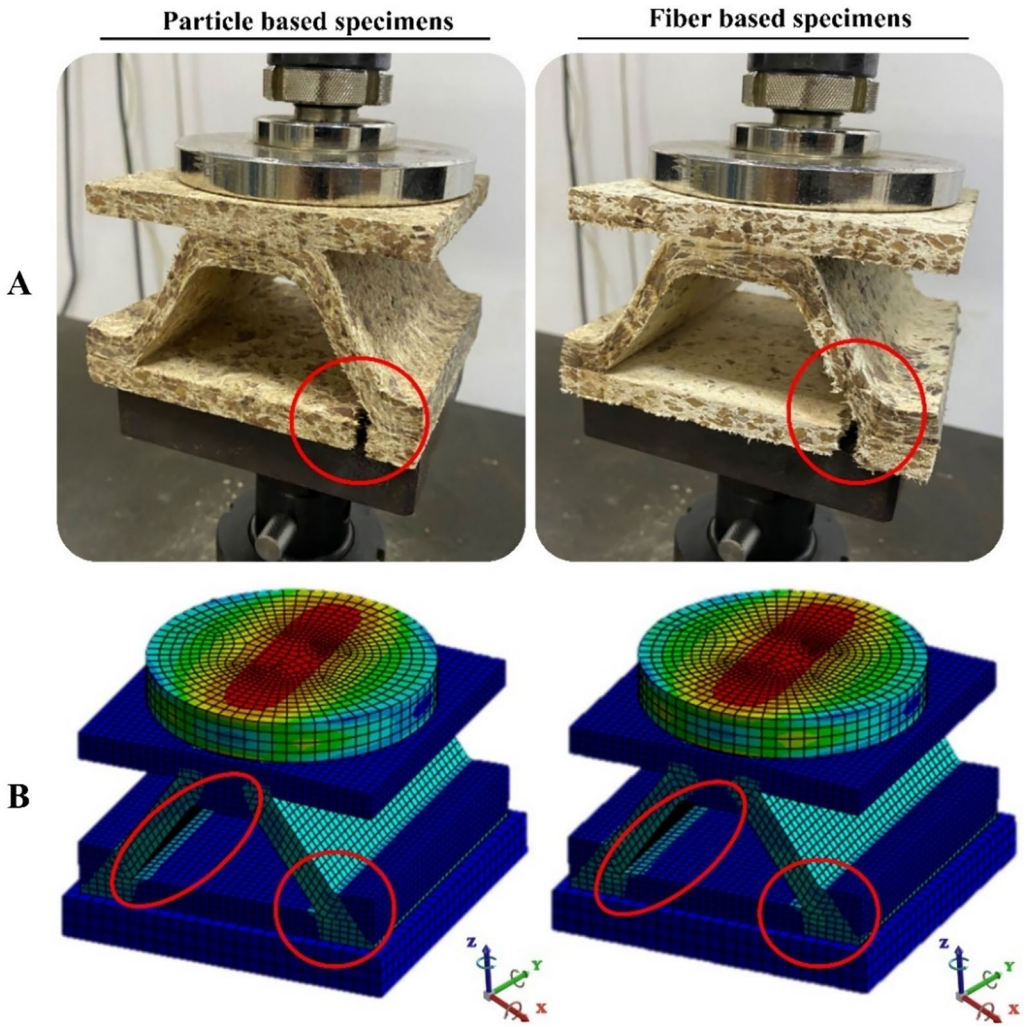

Fig. 8 Failure map of flatwise compression, **A** Experimental test, **B** Theoretical test

balsa wood waste, TOCS claimed to be a proper alternative for wooden species [45]. However, a different failure mode was observed (Fig. 8A) for these specimens compared with corrugated panels. It was found that the bonding between the core layer and surface layers helped the slope area of corrugated to provide a static condition and consequently transferred the stress to the bottom layer. Hence, in both PBP and FBP, the bottom layers close to the bonding area ripped by the applied tension, whereas the slope area of corrugated was undamaged. It should be noted that in some FBP specimens, a negligible crack was observed at the slope area of corrugated. These findings are aligned with the results of FEA (equivalent (von Mises) stress), as shown in Fig. 8B, there is a strip of mesh with a higher tension (green color).

Fastener properties

The design of structural members when using this type of panel may be determined by the fastener connections [46]. Consequently, having basic information regarding the mentioned properties may be helpful for future research and development. Several factors could affect screw holding resistance, including screw type and diameter, pilot hole size, screw penetration depth, and direction, the size of raw materials, apparent bulk density, shear strength, and IB properties [47, 48]. The measured FSW resistance indicated a similar value for both PBP (2249 N with a COV% of 7.8) and FBP (2204 N with a COV% of 9.5) as shown in Table 5.

The mean values and test setup for dowel-bearing tests are presented in Table 5**.** This test was carried out in two directions (vertical and horizontal to corrugated structure). Based on the results, FBP specimens indicated a higher dowel bearing in both directions. The maximum

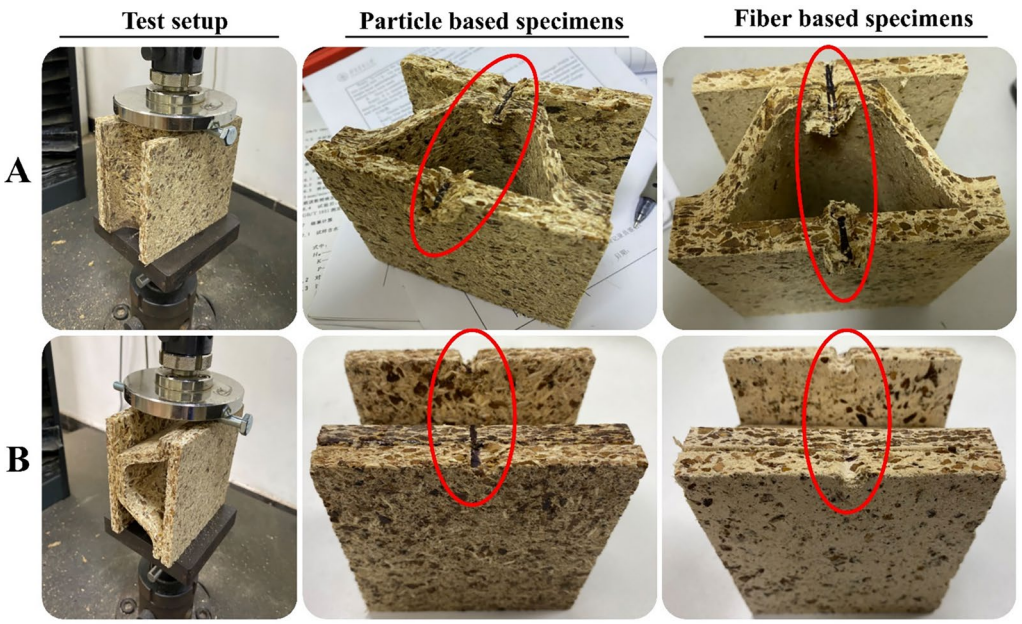

Fig. 9 Test setup and failure map of dowel-bearing test, **A** Vertical to corrugated, **B** Horizontal to corrugated

force for vertical dowel bearing (Fig. 9A) was 6853 N for PBP and 8076 N for FBP specimens. In addition, the horizontal dowel bearing indicated a value of 2826 for PBP and 3271 N for FBP specimens. The failure mechanism after removing the load is shown in Fig. 9B. The vertical load indicated a normal trend, with increasing the load, the dowel was penetrated in samples deeper until failure happened. On the other hand, the horizontal samples had a slight delamination in the bottom layer. The applied load caused a break in the glue line resulting in the separation of layers. This phenomenon appeared in both panel types and a simple solution for that is increasing the glue usage for bonding the core layer to surfaces or using some other glues such as polyurethane based [41].

Specific energy absorption analysis

The results of SEA for specimens under bending and compression tests are listed in Table 6. It was observed that PBP could absorb more energy in both tests. In detail, the specimens prepared in the longitudinal direction indicated a higher SEA. This value for PBP and FBP was 6.94 and 6.91 J/g, while transverse specimens had a value of 5.56 and 4.54 J/g, respectively. The energy absorption capability of a sandwich panel is related to the failure mechanisms of the core and surface layers. The failure map of specimens based on fibers revealed a weaker slope in the core layer (Fig. 7). Hence, lower SEA values were expected. In addition, results for the compression test showed a SEA value of about 40% higher for PBP specimens.

Conclusions

This study investigated the mechanical properties of trapezoidal corrugated panels using agricultural waste (TOCS) in combination with Poplar particles and fibers. Experimental findings indicated that a mixture of TOCS with Poplar particles yielded superior mechanical properties, which were supported by numerical FEA results. Specifically, Poplar particle-based panels exhibited enhanced bending stiffness, maximum bending

Table 6 The mean value of energy absorption of bending and compression tests

Test type	Particle-based specimens			Fiber-based specimens		
	Weight (g)	F_{max} (N)	SEA (J/g)	Weight (g)	F_{max} (N)	SEA (J/g)
BS (transverse)	838	1596	5.56	830	1430	4.54
BS (longitudinal)	826	1664	6.94	829	1566	6.91
Compression test	356	7659	48.4	349	5279	33.8

BS is bending strength test

moments, flatwise compression strength, and resistance to screw withdrawal. However, fiber-based panels showed stronger dowel-bearing strength. Analysis of failure maps underscored the predictive capability of FEA in identifying failure regions. Overall, the study suggests that the combination of TOCS with Poplar particles offers a promising avenue for producing lightweight, eco-friendly panels with improved mechanical performance, aligning with sustainability objectives.

Abbreviations

CE	Circular economy
TOCS	Tea oil Camellia shell
FEA	Finite element analysis
pMDI	Polymeric methylene diisocyanate
PVA	Polyvinyl acetate
PBP	Particle-based panel
FBP	Fiber-based panel
MOR	Modulus of rupture
MOE	Modulus of elasticity
IB	Internal bonding
FSW	Face screw withdrawal resistance
SEA	Specific energy absorption

Acknowledgements
This study was financially supported by the Bureau of Guangdong Forestry (Project No.2020KJCX008) and the National Natural Science and Foundation of China (Project No.32271783).

Author's contributions
K.CH.CH: Methodology, investigation, performed the experiments and analyzed, formal analysis, and writing—original draft preparation; J.T: Performed the experiments and analyzed, resource; Y.Z: Formal analysis, review, and editing; Y.L: Validation, review and editing; CH.H: Supervision, project administration and funding acquisition. All authors have read and agreed to the final manuscript.

Funding
Bureau of Guangdong Forestry, 2020KJCX008, Chuanshuang Hu, National Natural Science and Foundation of China, 32271783, Chuanshuang Hu.

Data availability
Data will be made available on request.

Declarations

Competing interests
The authors declare that they have no known competing financial interests or personal relationships that could have appeared to influence the work reported in this paper.

Received: 17 January 2024 Accepted: 3 June 2024
Published online: 02 July 2024

References

1. Faidzi MK, Abdullah S, Abdullah MF, Azman AH, Hui D, Singh SSK (2021) Review of current trends for metal-based sandwich panel: failure mechanisms and their contribution factors. Eng Fail Anal 123:105302. https://doi.org/10.1016/j.engfailanal.2021.105302
2. Sayahlatifi S, Rahimi GH, Bokaei A (2020) The quasi-static behavior of hybrid corrugated composite/balsa core sandwich structures in four-point bending: experimental study and numerical simulation. Eng Struct 210:110361. https://doi.org/10.1016/j.engstruct.2020.110361
3. Jantawee S, Lim H, Li M, Oh JK, Pasztory Z, Cho H, Srivaro S (2023) Developing structural sandwich panels for energy-efficient wall applications using laminated oil palm wood and rubberwood-based plywood/oriented strand board. J Wood Sci. https://doi.org/10.1186/s10086-023-02109-x
4. Shalbafan A, ChoupaniChaydarreh K, Welling J (2016) Development of a one-step process for production of foam core particleboards using rigid polyurethane foam. BioResources 11:9480–9495
5. Hao J, Wu X, Oporto G, Liu W, Wang J (2020) Structural analysis and strength-to-weight optimization of wood-based sandwich composite with honeycomb core under three-point flexural test. Eur J Wood Wood Prod 78:1195–1207. https://doi.org/10.1007/s00107-020-01574-1
6. Benzidane MA, Benzidane R, Hamamousse K, Adjal Y, Sereir Z, Poilâne C (2022) Valorization of date palm wastes as sandwich panels using short rachis fibers in skin and petiole "wood" as core. Ind Crops Prod 177:114436. https://doi.org/10.1016/j.indcrop.2021.114436
7. Wang X, Shi X, Meng Q, Hu Y, Wang L (2020) Bending behaviors of three grid sandwich structures with wood facing and jute fabrics/epoxy composites cores. Compos Struct 252:112666. https://doi.org/10.1016/j.compstruct.2020.112666
8. Chanda A, Kim NK, Bhattacharyya D (2021) Manufacturing and characterisation of wood-veneer sandwich panels with flame-retardant composite cores. Compos Commun 27:100870. https://doi.org/10.1016/j.coco.2021.100870
9. Lakreb N, Şen U, Toussaint E, Amziane S, Djakab E, Pereira H (2023) Physical properties and thermal conductivity of cork-based sandwich panels for building insulation. Constr Build Mater. https://doi.org/10.1016/j.conbuildmat.2023.130420
10. Shaban M, Alibeigloo A (2020) Global bending analysis of corrugated sandwich panels with integrated piezoelectric layers. J Sandw Struct Mater 22:1055–1073. https://doi.org/10.1177/1099636218780172
11. Smardzewski J (2019) Wooden sandwich panels with prismatic core—energy absorbing capabilities. Compos Struct 230:111535. https://doi.org/10.1016/j.compstruct.2019.111535
12. Mohammadabadi M, Yadama V, Dolan JD (2021) Evaluation of wood composite sandwich panels as a promising renewable building material. Materials (Basel) 14:1–14. https://doi.org/10.3390/ma14082083
13. Kavermann SW, Bhattacharyya D (2019) Experimental investigation of the static behaviour of a corrugated plywood sandwich core. Compos Struct 207:836–844. https://doi.org/10.1016/j.compstruct.2018.09.094
14. Jiao P, Borchani W, Soleimani S, McGraw B (2017) Lateral-torsional buckling analysis of wood composite I-beams with sinusoidal corrugated web. Thin-Walled Struct 119:72–82. https://doi.org/10.1016/j.tws.2017.05.025
15. Barbirato GHA, Junior WEL, Martins RH, Miyamoto B, Ho TX, Sinha A, Fiorelli J (2022) Sandwich OSB trapezoidal core panel with balsa wood waste. Waste Biomass Valoriz 13:2183–2194. https://doi.org/10.1007/s12649-021-01660-2
16. Lao WL, Chang L (2023) Comparative life cycle assessment of medium density fiberboard and particleboard: a case study in China. Ind Crops Prod 205:117443. https://doi.org/10.1016/j.indcrop.2023.117443
17. Lee SH, Lum WC, Boon JG, Kristak L, Antov P, Pedzik M, Rogozinski T, Taghiyari HR, Lubis MAR, Fatriasari W, Yadav SM, Chotikhun A, Oizzi A (2022) Particleboard from agricultural biomass and recycled wood waste: a review. J Mater Res Technol 20:4630–4658. https://doi.org/10.1016/j.jmrt.2022.08.166
18. Liu X, Wu Y, Gao Y, Jiang Z, Zhao Z, Zeng W, Xie M, Liu S, Liu R, Chao Y, Nie S, Zhang A, Li C, Xiao Z (2022) Valorization of *Camellia oleifera* oil processing byproducts to value-added chemicals and biobased materials: a critical review. Green Energy Environ 9:28–53. https://doi.org/10.1016/j.gee.2022.12.002
19. Choupani Chaydarreh K, Lin X, Guan L, Yun H, Gu J, Hu C (2021) Utilization of tea oil camellia (*Camellia oleifera* Abel.) shells as alternative raw materials for manufacturing particleboard. Ind Crops Prod 161:113221. https://doi.org/10.1016/j.indcrop.2020.113221
20. Choupani Chaydarreh K, Lin X, Guan L, Hu C (2022) Interaction between particle size and mixing ratio on porosity and properties of tea oil camellia (*Camellia oleifera* Abel.) shells-based particleboard. J Wood Sci 68:43. https://doi.org/10.1186/s10086-022-02052-3
21. Słonina M, Dziurka D, Smardzewski J (2023) Failure mechanism map for bending wood-based honeycomb sandwich beams with

starch-impregnated core. Compos Struct 310:16749. https://doi.org/10.1016/j.compstruct.2023.116749
22. Taghizadeh SA, Farrokhabadi A, Liaghat G, Pedram E, Malekinejad H, Mohammadi SF, Ahmadi H (2019) Characterization of compressive behavior of PVC foam infilled composite sandwich panels with different corrugated core shapes. Thin-Walled Struct 135:160–172. https://doi.org/10.1016/j.tws.2018.11.019
23. Zhou K, You T, Gong D, Zhou J (2023) A unified dynamic model and vibration suppression for moving corrugated sandwich panels with general boundaries. Thin-Walled Struct 193:111248. https://doi.org/10.1016/j.tws.2023.111248
24. Rong Y, Liu J, Luo W, He W (2018) Effects of geometric configurations of corrugated cores on the local impact and planar compression of sandwich panels. Compos Part B Eng 152:324–335. https://doi.org/10.1016/j.compositesb.2018.08.130
25. ASTM D1554 (2016) Standard terminology relating to wood-base fiber and particle panel materials. In: Annual Book of ASTM Standards. ASTM, Philadelphia, Pennsylvania, USA
26. ASTM D1037 (2012) Standard test methods for evaluating properties of wood-base fiber and particle panel materials. In: Annual Book of ASTM Standards. ASTM, Philadelphia, Pennsylvania, USA
27. ASTM D3044 (2011) Standard test method for shear modulus of wood-based structure panels. In: Annual Book of ASTM Standards. ASTM, Philadelphia, Pennsylvania, USA
28. ASTM D3043 (2011) Standard test methods for structural panels in flexure. In: Annual Book of ASTM Standards. ASTM, Philadelphia, Pennsylvania, USA
29. ASTM C393 (2012) Standard test method for core shear properties of sandwich constructions by beam flexure. In: Annual Book of ASTM Standards. ASTM, Philadelphia, Pennsylvania, USA
30. ASTM D143 (2014) Standard test methods for small clear specimens of timber. In: Annual Book of ASTM Standards. ASTM, Philadelphia, Pennsylvania, USA
31. ASTM D5764 (2007) Standard test method for evaluating doerl-bearing strength of wood and wood-based products. In: Annual Book of ASTM Standards. ASTM, Philadelphia, Pennsylvania, USA
32. ASTM D1761 (2000) Standard test methods for mechanical fasteners in wood. In: Annual Book of ASTM Standards. ASTM, Philadelphia, Pennsylvania, USA
33. Baharin MS, Abdullah S, Singh SSK, Faidzi MK (2022) Computational fatigue failure analysis of magnesium alloy core structure inside the metal sandwich panels under constant spectrum loadings. Eng Fail Anal 136:106194. https://doi.org/10.1016/j.engfailanal.2022.106194
34. Rajput A, Sunny MR, Sarkar A (2023) Optimization of honeycomb parameters of sandwich composites for energy and specific energy absorption using particle swarm optimization. Mar Struct 92:103498. https://doi.org/10.1016/j.marstruc.2023.103498
35. Wilczyński A, Kociszewski M (2011) Determination of elastic constants of particleboard layers by compressing glued layer specimens. Wood Res 56:77–92
36. Cai Z, Senalik CA, Ross RJ (2021) Chapter 12: Mechanical properties of wood-based composite materials. In: Wood handbook—wood as an engineering material. USDA—Gen Tech Rep 15
37. Korai H, Kojima Y, Suzuki S (2015) Bending strength and internal bond strength of wood-based boards subjected to various exposure conditions. J Wood Sci 61:500–509. https://doi.org/10.1007/s10086-015-1494-7
38. Choupani Chaydarreh K, Lin X, Dandan L, Zhang W, Guan L, Hu C (2022) Developing 3-layer tea oil camellia (*Camellia oleifera* Abel.) shells-based particleboard with systematic study on particle geometry and distribution. Ind Crops Prod 179:114682. https://doi.org/10.1016/j.indcrop.2022.114682
39. ANSI A208.1 (2016) American national standard for particleboard. Composite panel association, Leesburg, Virginia, USA
40. Halicka A, Ślósarz S (2022) Analysis of behavior and failure modes of timber beams prestressed with CFRP strips. Compos Struct 301:116171. https://doi.org/10.1016/j.compstruct.2022.116171
41. Pozzer T, Gauss C, Ament Barbirato GH, Fiorelli J (2020) Trapezoidal core sandwich panel produced with sugarcane bagasse. Constr Build Mater 264:120718. https://doi.org/10.1016/j.conbuildmat.2020.120718
42. Oliveira PR, May M, Panzera TH, Hiermaier S (2022) Bio-based/green sandwich structures: a review. Thin-Walled Struct 177:109426. https://doi.org/10.1016/j.tws.2022.109426
43. Singh N, Rana A, Badhotiya GK (2021) Raw material particle terminologies for development of engineered wood. Mater Today Proc 46:11243–11246. https://doi.org/10.1016/j.matpr.2021.02.616
44. Wang D, Wang L, Liu Y, Tan B, Liu Y (2020) Failure mechanism investigation of bottom plate in concrete box girder bridges. Eng Fail Anal 116:104711. https://doi.org/10.1016/j.engfailanal.2020.104711
45. Barbirato GHA, Junior WEL, Martins RH, Soriano J, Fiorelli J (2022) Experimental evaluation and numerical modeling of the mechanical performance of OSB sandwich panels manufactured with trapezoidal core. Constr Build Mater 326:126721. https://doi.org/10.1016/j.conbuildmat.2022.126721
46. Lathuillière D, Bléron L, Descamps T, Bocquet JF (2015) Reinforcement of dowel type connections. Constr Build Mater 97:48–54. https://doi.org/10.1016/j.conbuildmat.2015.05.088
47. Choupani Chaydarreh K, Li Y, Lin X, Zhang W, Hu C (2023) Heat transfer efficiency and pMDI curing behavior during hot-pressing process of tea oil camellia (*Camellia Oleifera* Abel.) shell particleboard. Polymers 15(4):959. https://doi.org/10.3390/polym15040959
48. Farajollah Pour M, Hatefnia H, Dorieh A, Valizadeh Kiamahalleh M, Mohammadnia Afrouzi Y (2022) Research on medium density fiberboard (MDF) behavior against screw axial withdrawal: Impact of density and operational variables. Structures 39:194–206. https://doi.org/10.1016/j.istruc.2022.03.025

Publisher's Note